

pubs.acs.org/JPCA Article

Parametrization of the PM7 Semiempirical Quantum Mechanical Method for Silver Nanoclusters

Qiwei Sun and Rebecca L. M. Gieseking*



Cite This: https://doi.org/10.1021/acs.jpca.2c05782



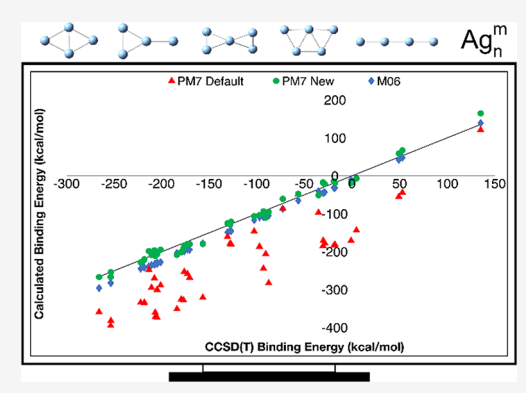
ACCESS

III Metrics & More

Article Recommendations

SI Supporting Information

ABSTRACT: Semiempirical quantum mechanical methods (SEQMs) are widely used in computational chemistry because of their low computational cost, but their accuracy depends on the quality of the parameters. The neglect of diatomic differential overlap method PM7 is among the few SEQMs that contain parameters for Ag, but the experimental reference data was insufficient to obtain reliable parameters in the original parametrization. In this work, we reparametrize the PM7 parameters for Ag to accurately reproduce the ground-state potential energy surfaces of Ag clusters. Since little experimental data is available, we use reference data obtained from the ab initio method CCSD(T). The resulting parameters significantly reduce the errors in binding energies, energies required to displace clusters along their normal modes, and relative energies of isomers compared to the default PM7 Ag parameters.



1. INTRODUCTION

Atomically precise silver clusters have been widely studied in recent years and have shown promise for applications in catalysis, 1-3 energy conversion, 1,4,5 and biomedical technology. 6-8 The utility of Ag nanoclusters for these applications is limited by the lack of understanding of their structureproperty relationships.9 Quantum mechanical modeling has been proven effective as a complement to experiments to provide insights into structure-property relationships in Ag clusters. 10,11 Many of the Ag nanoclusters studied experimentally contain 10-100 metal atoms, 1,4,6 and the cluster dynamics have a large effect on their suitability for applications. $^{12-15}$ For such large systems, high-level ab initio quantum mechanical methods are too computationally expensive to be feasible. Although density functional theory (DFT) has been widely used for metal nanoclusters, 10,11,16,17 DFT is challenging to use for applications like catalyst design due to the large number of possible structures in highly dynamic environments. 11 Lower-cost computational methods with sufficient accuracy to predict structure-property relationships will facilitate modeling of these nanoclusters to gain the chemical insight needed to design structures for various

Semiempirical quantum mechanical methods (SEQMs) are methods simplified from Hartree–Fock (HF), which allows them to capture quantum mechanical properties at greatly reduced computational cost. Within SEQMs, the computationally intensive three-center and four-center integrals are typically set to zero, and the remaining integrals are simplified using empirically determined parameters to obtain accurate results at a low cost. Typical SEQMs have a computational cost

that scales with the number of atoms N as $O(N^2)$, 19 whereas DFT typically scales as $O(N^3)^{20}$ and the coupled cluster theory CCSD(T) scales as $O(N^7)$. Since SEQMs are quantum mechanical, they are much more versatile than classical molecular mechanics models. With suitable parameters, SEQMs can reproduce important chemical properties such as noncovalent interactions, 19,21 dipole moments, 22 and proton transfer energetics 23 accurately enough for routine applications at several orders of magnitude lower computation cost than DFT.

Despite the potential advantages of SEQMs, there has been relatively little work toward developing accurate parameters for transition metals like Ag. We have recently parametrized the INDO/S SEQM to accurately predict the excited-state properties of Ag clusters; ^{24–26} however, since INDO/S was developed specifically for excited-state properties, these parameters are not suitable for ground-state properties. SEQMs within the OMx family have very high accuracy but have not been extended beyond a small handful of main-group elements. ^{27,28} In addition to the HF-based SEQMs, the semiempirical tight-binding approximation to DFT, known as DFTB, ²⁹ has been parametrized for metals like Ag and Au. ³⁰ DFTB is in good agreement with typical DFT functionals in predicting structural properties for Ag clusters like the

Received: August 12, 2022 Revised: August 25, 2022



transition from 2D to 3D cluster geometries and the energetic ordering of isomers. Time-dependent (TD) DFTB shows semiquantitative agreement with TD-DFT in the shapes of the absorption spectra and trends in excited-state energies for Ag nanorods. However, since DFTB is derived from the PBE functional, it inherits many of the limitations of GGA functionals, such as the underestimation of Pauli repulsion. The extended semiempirical tight-binding method GFN2-xTB is based on DFTB2 and is broadly parametrized to include all elements up to radon. GFN2-xTB has been shown to be more accurate than existing HF-based SEQMs in predicting geometries and reaction energies of transition metal complexes, the shown to be more accurate that the energies of transition metal complexes, the shown to be metal clusters.

Several HF-based SEQMs within the neglect of diatomic differential overlap (NDDO) class, PM6 and PM7, include parameters for transition metals; 36,37 however, the PM7 parameters for Ag are known to be inaccurate because of insufficient experimental reference data.³⁷ PM7 shares its basic mathematical structure with other NDDO methods: only the valence electrons are treated explicitly, and all one-electron integrals involving three centers, all two-electron integrals involving three or four centers, and two-center two-electron integrals except those of the Coulomb type are neglected. However, because of the sparse reference data, the accuracy in heat of formation for Ag containing solids in PM7 (MAE: 33.81 kcal/mol, for 10 solids)³⁸ is very low compared to organic compounds (MAE: 6.3 kcal/mol).³⁹ Although PM7 was parametrized for ground states, we have shown that the current parameters also overestimate the excited-state energies for the Ag₂₀ cluster by nearly 4 eV.⁴⁰ Reparametrization of NDDO methods has greatly improved accuracy for other metals, including Na in PM3, ⁴¹ Ru in PM6, ⁴² and lanthanide elements in PM7. ⁴³ Thus, reparametrization of PM7 is likely to substantially improve its accuracy for Ag clusters.

Here, we parametrize PM7 for Ag, focusing specifically on obtaining parameters that recreate the ground-state potential energy surfaces (PESs) of bare Ag clusters. Since there is insufficient experimental reference data available, our reference data is obtained from the ab initio method CCSD(T) for clusters of 2–7 Ag atoms and includes both equilibrium and displaced geometries to map the PES. Our parametrization method is based on a genetic algorithm. The resulting Ag parameters show significant improvement relative to the default PM7 parameters for the binding energies, energy changes upon displacement, and relative energies of isomers of Ag clusters. These results demonstrate that PM7 is capable of yielding accurate energies and PESs of a noble metal, and our methodology is possible to extend to the parametrization of other elements.

2. COMPUTATIONAL METHODS

2.1. Calculations Using Computational Chemistry Software. The equilibrium geometries of Ag_n clusters with different sizes $(2 \le n \le 7)$ and charges (-1, 0, and 1) were determined by performing geometry optimizations using density functional theory (DFT) with the B3LYP functional 44,45 with Grimme's D3 dispersion correction 46 and the cc-pVDZ-PP basis set. $^{47-49}$ To construct a library of equilibrium geometries, many initial geometries were constructed and optimized; the resulting geometries were screened to remove duplicate geometries. Vibrational frequencies were computed to confirm the absence of imaginary frequencies.

Because Ag_n clusters typically have filled d bands, all computations were performed with either a singlet spin for clusters with an even number of electrons or a doublet spin for clusters with an odd number of electrons.

The reference data for parametrization was obtained by computing the single point energies (SPEs) of the Ag_n clusters using coupled cluster with singles and doubles with perturbative triples (CCSD(T))⁵⁰ and the aug-cc-pVDZ-PP basis set^{47–49} with the zeroth order DKH scalar relativistic correction (DKH0).⁵¹ These calculations were performed for all of the B3LYP/cc-pVDZ-PP-optimized geometries. In addition, to account for their ground-state PESs, SPEs were computed at the same level of theory for geometries of the Ag clusters displaced along their normal modes. For Ag, clusters with $n \le 5$, all normal modes were used to generate displaced geometries; for $6 \le n \le 7$, six modes were chosen with a distribution of vibrational frequencies. For each mode, SPEs were computed for 7-9 displacements, roughly equally divided between displacements in positive and negative directions. The default displacements ranged from ± 0.1 to ± 1.0 Å; this range was modified for each mode to ensure that the largest displacement in each direction resulted in an energy change of at least 0.5 eV but no more than 10 eV relative to the equilibrium geometry. If the ± 1.0 Å displacement exceeded this range, then this data point was excluded and additional geometries at smaller displacements were added to keep the number of displacements consistent with the other modes; if the ± 1.0 Å displacement fell below this range, then displacements up to ± 1.5 Å were added.

SPE calculations for the equilibrium geometries were also performed using the M06 functional with the Stuttgart relativistic small core effective core potential basis set ECP28MWB, which has been used previously for Ag clusters. All DFT and CCSD(T) calculations were performed using Gaussian 16. The unrestricted Hartree–Fock (UHF) framework was used for all open-shell systems. Annihilation of the first spin contaminant resulted in $\langle s^2 \rangle$ values of 0.75–0.77 for the doublet systems (initial guess of $\langle s^2 \rangle = 0.75$).

SPEs were computed for all equilibrium and displaced geometries using the semiempirical PM6³⁶ and PM7³⁷ calculations using the MOPAC2016 software package. For calculations using non-default PM7 parameters, the modified parameters were read into MOPAC2016 from an additional input file. The UHF framework was used for all open-shell systems in semiempirical calculations. Computation of spin contaminants is not implemented in MOPAC2016. Geometry optimizations performed with semiempirical methods were performed in MOPAC2016 using the default optimization procedure. The root-mean-square deviation (RMSD) of a PM7-optimized geometry with respect to the reference geometry was computed using the Kabsch algorithm, in which the two clusters are recentered and rotated unto each other to get the minimum RMSD in the atomic positions. ^{57,58}

2.2. Reference Properties and Error Functions. To assess the accuracy of the parameters, three reference properties were defined: (1) binding energy, (2) displacement energy, and (3) relative energy of isomers. The raw SPEs E_{SPE} were converted to binding energies E_B using the formula:

$$E_B(Ag_n) = E_{SPE}(Ag_n) - n \times E_{SPE}(Ag_1)$$
(1)

where n is the number of Ag atoms. This conversion is applied to all level of theories (CCSD(T), DFT, and PMx). We note that our use of binding energy as a reference property differs

from the heat of formation used as a reference property in previous PM6/PM7 parametrizations since computing a true heat of formation at the CCSD(T) level would require corrections that are poorly defined for non-equilibrium geometries.

To assess the accuracy of the PESs, we define the displacement energy (ΔE_D) as the difference between the binding energy of a displaced geometry $(E_{B, disp})$ and its corresponding equilibrium geometry $(E_{B, ea})$:

$$\Delta E_D = E_{B,disp} - E_{B,eq} \tag{2}$$

We also use the energy difference between structural isomers as a reference property. The relative energy ΔE_R was defined as the energy difference between isomer n ($n \ge 2$) and a selected isomer 1 among clusters with the same chemical formula:

$$\Delta E_{R,isomer\ n} = E_{B,isomer\ n} - E_{B,isomer\ 1} \tag{3}$$

For each reference data point, the error ϵ was defined as the difference between the semiempirical value and the CCSD(T) value. The error function for a particular parameter set was computed as a weighted root-mean-square error (RMSE) defined as

weighted RMSE =
$$\sqrt{\frac{\sum_{i=1}^{n} c_i \epsilon_i^2}{\sum_{i=1}^{n} c_i}}$$
 (4)

where the weight c was set to 1.0 for all binding energies, 4.0 for displacement energies, and 80.0 for relative energies between isomers unless noted otherwise.

To assess the accuracy of the parameter sets, we also calculated the weighted mean signed error (MSE) defined as

weighted MSE =
$$\frac{\sum_{i=1}^{n} c_i \epsilon_i}{\sum_{i=1}^{n} c_i}$$
 (5)

and the weighted mean absolute error (MAE) defined as

weighted MAE =
$$\frac{\sum_{i=1}^{n} c_i |\epsilon_i|}{\sum_{i=1}^{n} c_i}$$
 (6)

- **2.3. Parametrization Procedure.** The parametrization procedure is based on a modified genetic algorithm, in which a population of candidate solutions to an optimization problem is gradually evolved toward better solutions. In this case, the optimization problem is minimizing the RMSE defined earlier, and the candidate solutions are the values of the PM7 parameters. The parametrization code for this algorithm was developed in-house and uses the following algorithm:
 - Initial parameter sets (points in parameter space) are constructed by reading manually input values or by randomly generating parameter sets within an allowed range.
 - For each parameter set, the SPEs are computed at the PM7 level for all structures in the training set, and the RMSE is calculated based on those energies.
 - 3. The value of each parameter is normalized within a range from 0 to 1, and *k*-NN analysis is used to determine the nearest neighbors for all points. The number of nearest neighbors is set to 3 or square root of the number of existing points, whichever is greater. All points that have smaller RMSE values than all of their nearest neighbors are selected as low-error points. After the first iteration, a second criterion is added to reduce

the computational time spent far from the global minimum: low-error points must also have RMSE values no more than twice the overall lowest RMSE among all points.

- 4. New parameter sets are generated based on the lowerror points. Two approaches are used:
 - a. Mutation: All parameters from the initial lowerror point are modified using random numbers. The new points must be closer to the initial lowerror point than the most distant point classified as a near neighbor in step 3, and this distance cutoff is scaled to 2/3 of the distance to the most distant near neighbor in later rounds. For each low-error point, the number of new points generated by mutation is either 5 times the number of parameters or the square root of the existing number of points, whichever is smaller.
 - b. Hybridization: For two low-error points, the values of all parameters are averaged. All pairs of low-error points are used to produce hybrids.
- 5. Steps 2-4 are repeated for a pre-set number of iterations, typically set to 10.

This approach enables us to explore broad regions of the high-dimensional parameter space with multiple local minima, which may be missed using a gradient-based method. Because PM7 includes 16 parameters, it is impractical to tune all 16 parameters at once. Instead, we followed an iterative procedure of tuning a subset of three or four parameters each time, cycling through subsets until all 16 parameters were tuned. The parameters were grouped in subsets by types, as in the original parametrization involving Ag in PM6: The first subset contained all three U parameters ($U_{\rm ss}$, $U_{\rm pp}$, and $U_{\rm dd}$), and the subsequent four subsets similarly contained the three β parameters, three ζ parameters, three ζ_n parameters, and the remaining four parameters. Parametrization of all subsets was repeated until the RMSE remained consistent between parametrization cycles.

During the parametrization process, penalties were added to the RMSE to ensure that the algorithm favored parameter sets with qualitatively correct chemical properties. The penalty for a failure to achieve convergence of the self-consistent field (SCF) procedure was set to 40,000 kcal/mol for binding energies and 10,000 kcal/mol for displacement energies. In the final parametrization round, a penalty of 100 kcal/mol was added if the displacement energy had opposite signs between the reference data and the calculated data (wrong curvature). The weights for the reference properties were also changed throughout the parametrization process. The weight of the binding energy was always set as 1.0. The weight of displacement energy was initially set as 3.0 and increased to 4.0 in later rounds to ensure the correct curvature of the PESs. The relative energy between structural isomers was only used as a reference parameter in the final parametrization round, with a weight of 80.0 because of the small number of equilibrium geometries in the reference data set.

3. RESULTS AND DISCUSSION

3.1. Geometries of Ag_n **Clusters.** The accuracy of semiempirical methods is limited by the availability of high-quality reference data used to fit the parameters. For Ag clusters, there is little experimental data available. Thus, to obtain accurate semiempirical methods, generating high-level

ab initio reference data is essential. We have constructed a library of 48 structures optimized at the B3LYP/cc-pVDZ-PP level of theory from Ag_2 to Ag_7 with charges of -1, 0, and +1. Many of these chemical formulas have multiple stable isomers; for each chemical formula, the lowest-energy structure at the B3LYP/cc-pVDZ-PP level is shown in Figure 1.

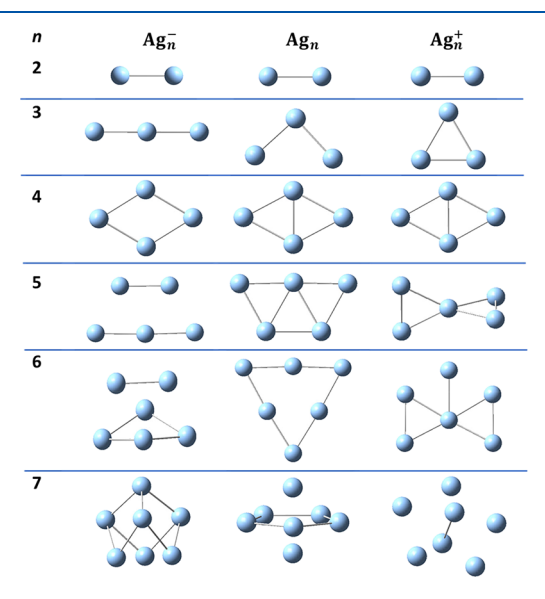


Figure 1. Structures of the most stable Ag_n^x clusters at the B3LYP/cc-pVDZ-PP level of theory.

In our parametrization, we prioritized obtaining not only accurate energies of the Ag_n clusters but also accurate PESs near the equilibrium geometry. To describe the PES, each cluster was displaced along its vibrational modes as described in Section 2. This resulted in a reference data set containing the CCSD(T)/aug-cc-pVDZ-PP energies of 2129 distinct geometries. For parametrization, this reference data was divided into two non-overlapping subsets: (1) a training set used during the parametrization cycles to fit the parameters and (2) a test set used to check the performance of the final parameters. The training set contains 1795 geometries as detailed in Table 1, 84% of the reference data. Based on the SPEs of all 1795 geometries, we derived three reference properties:

1. Binding energy of the cluster.

Table 1. Composition of the Training Set^a

n	Ag_n^-	Ag_n	Ag_n^+
2	1 (8)	1 (9)	1 (7)
3	2 (49)	1 (17)	1 (25)
4	2 (89)	2 (91)	2 (80)
5	2 (101)	1 (70)	3 (145)
6	6 (265)	4 (165)	5 (197)
7	2 (83)	6 (263)	3 (131)
sum of clusters	15	15	15
total geometries	45 (1795)		

^aThe number of equilibrium geometries with each chemical formula are in bold, and the total number of equilibrium and displaced geometries is in parentheses.

- 2. Displacement energy, defined as the energy difference between a geometry displaced along a normal mode and the corresponding equilibrium geometry.
- Isomer relative energy, defined as the energy difference between two equilibrium geometries with the same chemical formula.

For the 1795 geometries, the combination of these three reference properties produced a total of 3571 data points in the training set.

The test set contains 334 geometries that are not present in the training set. Three categories of geometries were selected to check for overfitting in different ways:

- 1. Equilibrium and all displaced geometries from three clusters that are not present in the training set: one Ag_4^- , one Ag_5^- , and one Ag_7^- (148 total geometries).
- 2. All displacements of 12 randomly picked normal modes from different clusters across all sizes and charges (95 total geometries).
- 3. Randomly chosen geometries from throughout the reference data set (91 total geometries).

3.2. Accuracy of New PM7 Parameters for Ag Clusters. To perform the parametrization, we used a modified genetic algorithm, and the parameters were tuned iteratively in small groups of three to four parameters for several rounds until their values converged. The details of the algorithm and procedure can be found in Section 2.3. Since the mathematical structure of the semiempirical PM7 Hamiltonian has been previously described in detail, ^{36,37} we summarize the default and new parameters for Ag in Table 2. The largest numerical

Table 2. List of Tunable Parameters for Ag in PM7

parameter	name in MOPAC	default value	new value	description
$U_{ m ss}$	USS	-92.2805	-93.1040	U parameters: one-
$U_{ m pp}$	UPP	29.2300	41.0328	center energies
$U_{ m dd}$	UDD	-82.3449	-168.8800	
$eta_{ extsf{s}}$	BETAS	-9.8508	-7.2305	β parameters:
$eta_{ m p}$	BETAP	-29.8947	-44.7294	resonance integrals
$eta_{ m d}$	BETAD	-63.6363	-65.2601	
$\zeta_{ m s}$	ZS	1.7930	1.8045	ζ parameters: orbital
$\zeta_{\rm p}$	ZP	2.5287	2.5139	exponents
$\zeta_{ m d}$	ZD	3.5248	3.5663	
$\zeta_{ m sn}$	ZSN	1.6198	1.6353	$\zeta_{\rm n}$ parameters:
$\zeta_{ m pn}$	ZPN	0.4397	0.4332	internal exponents
ζ_{dn}	ZDN	1.2102	1.1990	
$F_0(sd)$	F0SD	8.9878	9.0043	Slater-Condon
$G_2(sd)$	G2SD	4.7166	4.7414	parameters
AlpB_NN	ALPB_Ag	1.4894	1.5013	pair specific core-
XFac_NN	XFAC_Ag	0.1789	0.1854	core repulsion parameters

changes are to the U and β parameters, while the other parameters remain closer to their original values. We observed that the PM7 energy is much more sensitive to small numerical changes in parameters like ζ or Slater—Condon than to the U and β parameters, so it is unsurprising that these parameters vary within a much smaller range. We note that $U_{\rm pp}$ is positive in the new PM7 Ag parameters. This is consistent with the original formulation of PM7, in which the energy of the p orbitals in transition metals was raised to achieve accurate ground-state energies. ³⁷ Our parametrization also indicates

that $U_{\rm pp}$ indeed needs to be positive to obtain correct energies for Ag.

To demonstrate the improvements in the new parameters, we compare the accuracy to that of the default PM7 and PM6 for the training set (Table 3). The overall weighted errors were

Table 3. Error Statistics (kcal/mol) for the Full Training Set (Including All Three Reference Properties), Binding Energies, and Displacement Energies at the New PM7, Default PM7, PM6 Levels^b

training set overall weighted errors				
	new PM7	default PM7	PM6	
MSE	1.97	-22.37	23.78	
MAE	7.05	32.51	49.74	
RMSE	11.28	58.31	97.21	
no. of SCF failure	0	2	2 ^a	
binding energy only				
_	new PM7	default PM7	PM6	
MSE	0.12	-123.01	162.64	
MAE	10.00	123.43	177.56	
RMSE	14.06	132.71	220.81	
no. of SCF failure	0	2	2	
	displacement ene	rgy only		
	new PM7	default PM7	PM6	
MSE	3.24	-4.49	-4.45	
MAE	6.73	12.19	16.96	
RMSE	11.53	23.09	32.89	
no. of SCF failure	0	2	а	

^aSince one equilibrium structure had an SCF failure, the displacement energies for that cluster (45 data points) are undefined and excluded from the error statistics. ^bGeometries with SCF failures were excluded when computing the error statistics.

calculated relative to the CCSD(T)/aug-cc-pVDZ-PP energies using the same weights assigned in the final rounds of parametrization: 1.0 for binding energies, 4.0 for displacement energies, and 80.0 for relative energies between structural isomers. The rationale behind these weights is to augment the effect of properties with smaller numerical values and/or fewer data points. The number of data points for the binding energy and displacement energy is roughly equal, but the errors in the displacement energies are typically several times smaller than in raw binding energies because the displacement energies are differences between two binding energies. Since the relative energy of structural isomers only exists for equilibrium geometries, there are less than 40 total reference values, a factor of 40 fewer than the other reference properties, which justifies the much larger weight of 80.0. Structures that failed to reach SCF convergence with a given parameter set, i.e., SCF failures, are listed in the table but are not included in the error statistics.

These error statistics show that the new PM7 parameters perform significantly better than the default PM7 and PM6 parameters, reducing the overall error and eliminating SCF failures. For the overall weighted data set, the new parameters reduce RMSE and MAE by a factor of 5 relative to the default PM7 parameters. The MSE is also smaller by more than an order of magnitude, suggesting that the new parameters have less systematic over- or underestimation of energies. Since PM6 has known flaws in treating metals and crystalline solids, ^{37,59} it is unsurprising that its errors are larger than those

of the default PM7. PM6 also yielded an SCF failure for one of the Ag_7 equilibrium geometries, so the displacement energies for that cluster are undefined.

Next, we examine the error for each of the categories of reference data within the training set. Starting with the binding energies, both the default PM7 and PM6 produce errors on the order of 100-200 kcal/mol and cause two SCF failures. For the default PM7, the MSE and MAE have very similar magnitudes but opposite signs, which indicates that this method consistently underestimates binding energies for Ag clusters. For PM6, the MSE and MAE are similarly similar in magnitude but opposite in sign, indicating that PM6 consistently overestimates binding energies for Ag clusters by an average of 162 kcal/mol. These errors are far too large to obtain any meaningful binding energies for Ag clusters, which highlight the necessity of reparametrization; for comparison, the default PM7 parameters yield an MAE of 6.70 kcal/mol for carbon-containing molecules 60 and 11.97 kcal/mol for carboncontaining solids. 61 For the new Ag parameters, the RMSE is reduced to 14.06 kcal/mol, which is almost 10 times smaller than the default PM7 and 20 times smaller than PM6, and the MAE of 10.00 kcal/mol is on par with the errors in PM7 for well-parametrized elements like carbon. The MSE is only 0.12 kcal/mol, which indicates that the new parameters eliminate the systematic shift in the binding energy present for the default PM7 and PM6 methods. We note the errors for standard elements are based only on equilibrium geometries; since our training set also includes displaced geometries that are more challenging to reproduce, it is not surprising that our errors tend to be slightly larger than those for standard elements. Some representative examples of the performance of our new parameters for the binding energies of displaced geometries are shown in Figure S1.

To provide a more direct comparison to the standard elements, we also examine the error in binding energy for only the equilibrium geometries. We compare not only to the default PM7 and PM6 but also to DFT at the M06/ECP28MWB level; this functional has been shown to be one of the most accurate for the energetic properties of Ag clusters relative to CCSD(T). As shown in Figure 2, the default PM7 parameters consistently underestimate the binding

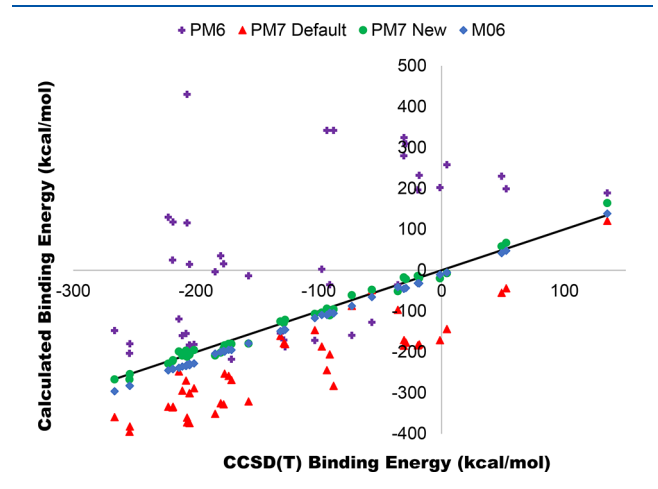


Figure 2. Binding energies of equilibrium geometries of the Ag_n clusters computed at the new PM7, default PM7, PM6, and M06/ECP28MWB levels relative to the reference data at the CCSD(T)/aug-cc-pVDZ-PP level.

energies, and the magnitude of the error is larger for the larger clusters that have more negative binding energies. PM6 consistently overestimates the binding energies, with larger magnitudes of errors than the default PM7. Both the default PM7 and PM6 have not only large average errors but also substantial scatter in the data that is not apparent from the numerical error statistics. In contrast, both M06/ECP28MWB and the new PM7 parameters generate binding energies that are much closer to the CCSD(T) reference data. M06/ECP28MWB consistently underestimates the binding energies, yielding an MSE of -19.00 kcal/mol and an MAE of 19.00 kcal/mol (Table 4). In contrast, the new PM7 yields binding

Table 4. Error Statistics (kcal/mol) for the Binding Energies of Equilibrium Geometries at the New PM7, Default PM7, PM6, and M06/ECP28MWB Levels^a

	new PM7	default PM7	PM6	M06
MSE	-2.48	-116.92	156.43	-19.00
MAE	8.22	116.92	173.40	19.00
RMSE	10.49	94.94	219.45	20.00
No. of SCF failures	0	0	1	0

^aGeometries with SCF failures were excluded when computing the error statistics.

energies both slightly higher and lower than the reference data, yielding an MSE of -2.48 kcal/mol and a larger MAE of 8.22 kcal/mol; this MAE is less than half the value obtained from DFT, showing that these parameters accurately reproduce the ground-state energy of these Ag clusters in their equilibrium geometries. Since this MAE is based only on the equilibrium geometries, it provides a more direct comparison to the values for other elements. The MAE of 8.22 kcal/mol is slightly larger than the MAE of carbon-containing molecules $(6.70 \text{ kcal/mol})^{60}$ but is within an acceptable range for a method with such a low computational cost.

For the equilibrium geometries, we also examine the accuracy of the relative energies between structural isomers (Table 5). Here, we apply a new definition for relative energy

Table 5. Error Statistics (Kcal/Mol) for the Relative Energies at the New PM7, Default PM7, PM6, and M06/ECP28MWB Levels^a

relative energy of equilibrium geometries				
new PM7 default PM7 PM6 M06				
MAE	3.66	14.00	34.60	0.64
RMSE	4.41	16.49	43.77	0.76
no. of SCF failure	0	0	1	0

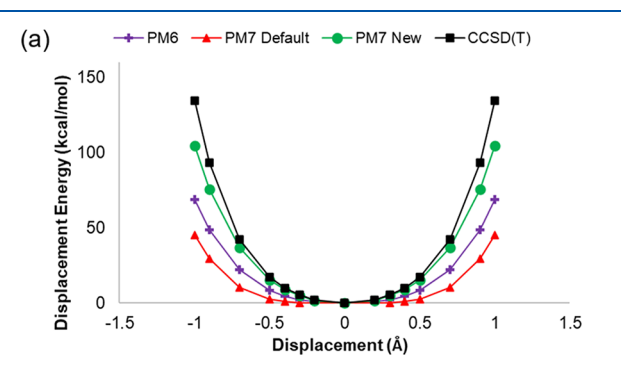
[&]quot;Geometries with SCF failures were excluded when computing the error statistics.

that is slightly different than the definition used during the parametrization runs (and in Table 3's overall weighted errors). To reduce bias in our statistics based on which isomer is selected as a reference point, the relative energy is defined as the difference between the energy of a certain isomer k and the average energy of all its isomers:

$$\Delta E'_{rela} = E_{B,isomer \ k} - \frac{\sum_{i=1}^{n} (E_{B,isomer \ i})}{n}$$
(7)

where n is the total number of isomers with the same chemical formula. Under this definition, the MSE of relative energies must be zero, so the MSE for relative energies is not listed in Table 5. M06/ECP28MWB performs quite well for relative energies with an MAE of only 0.64 kcal/mol; this error is lower than that seen previously for other DFT functionals, which yield MAEs on the order of 2-4 kcal/mol for relative energies in Ag⁶³ or Au⁶⁴ clusters up to eight metal atoms. Our new PM7 parameters produce an MAE of 3.66 kcal/mol for relative energies, which is larger than that of M06 but comparable to many other DFT functionals. The low error means our new parameters perform acceptably well in capturing the subtle energy changes caused by conformational differences among the Ag_n clusters. As for the other reference properties, the default PM7 and PM6 yield errors that are too large to have useful predictive power.

To evaluate the ability of the methods to produce accurate potential energy surfaces, we examine the displacement energies along the vibrational normal modes (Table 3). Because the displacement energies are differences between the energies of two related structures, the magnitude of the errors is significantly smaller than for the binding energies. As for the other reference properties, the default PM7 and PM6 produce relatively large errors for the displacement energies. The new PM7 parameters are able to reduce the MAE and RMSE to half their values from the default PM7 parameters and a little more than a third the error from PM6. The improvements in the displacement energies lead to a better description of the ground-state PESs of the Ag clusters; representative examples of this improvement are shown in Figure 3. Since these parameters produce the correct curvature of the PES around the equilibrium geometry, this suggests that



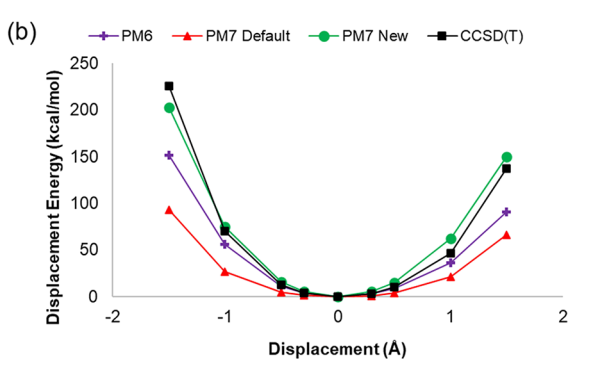


Figure 3. Potential energy surfaces of (a) symmetrical normal mode in Ag_5 and (b) asymmetrical normal mode in Ag_7^- at the new PM7, default PM7, and PM6 levels compared to the reference data at the CCSD(T)/aug-cc-pVDZ-PP level.

they will also yield reasonable optimized geometries. For most normal modes in the training set, the new PM7 parameters generally perform well when the displaced geometry is close to the equilibrium geometry but are less accurate for larger displacements where the displacement energy approaches the 231 kcal/mol (10 eV) cutoff. This can be seen by separating the data into structures with small and large displacement energies, with a cutoff of 50 kcal/mol (2.17 eV). As shown in Table 6, the structures with large displacement energies have

Table 6. Error Statistics (kcal/mol) for Binding Energy and Displacement Energy at the New PM7 Level, Decomposed in Structures with Large ($\Delta E_D > 50 \text{ kcal/mol}$) and Small ($\Delta E_D < 50 \text{ kcal/mol}$) Displacement Energies^a

binding energy			
	$\Delta E_D < 50 \text{ kcal/mol}$	$\Delta E_D > 50 \text{ kcal/mol}$	
MSE	0.51	-2.75	
MAE	8.55	17.95	
RMSE	11.39	23.74	
	displacement energy	,	
	ΔE_D < 50 kcal/mol	$\Delta E_D > 50 \text{ kcal/mol}$	
MSE	3.61	1.34	
MAE	4.81	18.05	
RMSE	8.21	23.41	

^aIn both data sets, the errors in binding energies include all equilibrium geometries.

significantly larger errors in both binding energy and displacement energies than the structures with small displacement energies.

We also examine the performance of the new PM7 parameters for subsets of the training set with common structural features: charge, spin, and size. This decomposition reveals whether the parameters perform acceptably well for all structures within the training set. We first examine the error statistics for Ag clusters with charges of 0, +1, and -1 (Table 7). The weights of all reference properties are the same as in the overall statistics from Table 3. For our new PM7 parameters, the RMSD ranges from 8.93 kcal/mol for the anionic clusters to 13.63 kcal/mol for the cationic clusters. Since all three charges have 15 total equilibrium geometries and quite similar numbers of total geometries in the training set, the differences in the errors are not due to unbalanced weighting of the charges and may instead reflect the ability of the mathematical formalism of PM7 to describe the electronic structures of these clusters. This is supported by the results from the default PM7 and PM6: both methods have their largest errors for the cationic clusters and the smallest for the anionic clusters. Across all three charges, the new PM7 parameters produce errors roughly a factor of five smaller than the default PM7 parameters and 5-10 times smaller than PM6, consistent with the results from the full training set.

We now examine the effects of spin. Since Ag atoms have a d¹⁰s¹ electron configuration, Ag clusters typically have few unpaired electrons; in this study, all systems with an even number of electrons were computed as singlets (closed shell) and all systems with an odd number of electrons were computed as doublets (open shell). All of the SCF failures in the default PM7 and PM6 were in open-shell systems (Table 8), which is unsurprising since open-shell systems are often more challenging to model. However, in the overall error

Table 7. Error Statistics (kcal/mol) for the Full Training Set at the New PM7, Default PM7, and PM6 Levels Decomposed by Cluster Charge^b

	charge 0		
	new PM7	default PM7	PM6
MSE	0.78	-22.16	38.15
MAE	6.94	36.67	55.91
RMSE	11.13	63.59	99.80
no. of SCF failure	0	0	2 ^a
	charge +1		
	new PM7	default PM7	PM6
MSE	3.63	-28.52	35.85
MAE	8.85	37.37	70.53
RMSE	13.63	67.67	129.72
no. of SCF failure	0	2	0
	charge —	l	
	new PM7	default PM7	PM6
MSE	1.77	-17.39	1.00
MAE	5.82	25.07	24.96
RMSE	8.93	41.69	43.45
no. of SCF failure	0	0	0

[&]quot;Since one equilibrium structure had an SCF failure, the displacement energies for that cluster (45 data points) are undefined and excluded from the error statistics. "Geometries with SCF failures were excluded when computing the error statistics.

Table 8. Error Statistics (kcal/mol) for the Full Training Set at the New PM7, Default PM7, and PM6 Levels Decomposed into Open-Shell and Closed-Shell Systems^b

	open shel	Í	
	new PM7	default PM7	PM6
MSE	1.83	-19.09	25.07
MAE	5.35	28.97	48.53
RMSE	8.90	53.51	93.69
no. of SCF failure	0	2	2 ^a
closed shell			
	new PM7	default PM7	PM6
MSE	2.17	-26.65	22.18
MAE	9.27	37.14	51.25
RMSE	13.78	64.03	101.43
no. of SCF failure	0	0	0

[&]quot;Since one equilibrium structure had an SCF failure, the displacement energies for that cluster (45 data points) are undefined and excluded from the error statistics. "Geometries with SCF failures were excluded when computing the error statistics.

statistic excluding the structures with SCF failures, the openshell systems surprisingly have lower error than the closed shell systems for all three methods. For our new PM7 parameters, the difference in the errors between open- and closed-shell systems is comparable to the difference in the errors between the different charges. The better performance for the openshell systems may be because there are a larger number of open-shell systems in the training set since Ag_6^- and Ag_7 have many isomers (Table 1).

To examine the effect of cluster size, we group the Ag clusters in the training set into two groups: small clusters with 2–4 atoms, and large clusters with 5–7 atoms (Table 9). The default PM7 and PM6 have smaller errors for the smaller clusters, which is unsurprising because these methods did not

Table 9. Error Statistics (kcal/mol) for the Full Training Set at the New PM7, Default PM7, and PM6 Levels Decomposed by the Cluster Size^b

	Ag_n , $2 \le n \le$	≤ 4	
	new PM7	default PM7	PM6
MSE	0.91	-16.42	3.54
MAE	8.94	26.05	28.02
RMSE	12.79	42.77	45.16
no. of SCF failure	0	2	0
	Ag_n , $5 \le n \le$	≤ 7	
	new PM7	default PM7	PM6
MSE	2.24	-23.83	28.93
MAE	6.59	34.09	55.26
RMSE	10.88	61.51	106.46
no. of SCF failure	0	0	2 ^a

^aSince one equilibrium structure had an SCF failure, the displacement energies for that cluster (45 data points) are undefined and excluded from the error statistics. ^bGeometries with SCF failures were excluded when computing the error statistics.

include Ag clusters in their parametrization training set. In contrast, our new PM7 parameters perform slightly better for the larger clusters. This is also unsurprising because the larger clusters have more isomers and more vibrational modes and thus are more prominently represented in the training set. The difference in errors between the large and small clusters is smaller than the differences seen between different charges and spins. This suggests that the new parameters may be capable of producing reasonable energies for clusters larger than those in the training set.

3.3. Performance of Parameters for the Test Set. To check our PM7 parameters for overfitting, we separated the data into a training set and a test set prior to parametrization, as detailed in Section 3.1. The test set contains three categories of data intended to check for overfitting in different ways: (1) all equilibrium and displaced geometries of several clusters, intended to test the applicability of the parameters to new structures; (2) all displaced geometries for certain normal modes, intended to test the accuracy of the parameters for new regions of potential energy space; and (3) individual displaced geometries not present in the training set. Because of the construction of the test sets, relative energies of isomers are not available, so the statistics were calculated using only binding energy (weight = 1.0) and displacement energy (weight = 4.0).

For the first category (new geometries), the weighted RMSE is 9.01 kcal/mol (Table 10), which is lower than the 11.28 kcal/mol RMSE from the training set (Table 3). We note that all three Ag clusters in this portion of the test set are all anionic but include both open- and closed-shell structures; the RMSE for this portion of the test set is consistent with the RMSE for

Table 10. Error Statistics (kcal/mol) for the Three Categories of the Test Set Using the New PM7 Parameters

	test set		
	new geometries	new normal modes	individual displacements
MSE	1.97	-0.64	1.24
MAE	5.17	5.75	5.45
RMSE	9.01	10.03	9.48
no. of SCF failure	0	0	0

anionic clusters in the training set (8.93 kcal/mol; Table 7). Since our full reference data set contains more anionic clusters than neutral or cationic clusters, selecting several anionic clusters to include in the test set instead of the training set allows for a nearly equal distribution of charges within the training set and thus minimizes unbalanced weighting of different charges during training. For the second category (new normal modes), the weighted RMSE is 10.03 kcal/mol, which is also slightly lower than the overall RMSE for the training set. For the third category (individual displacements), the RMSE is 9.48 kcal/mol, which is again smaller than the overall RMSE for the training set. We also note that the magnitudes of the errors are consistent across the three different categories inside the test set (MAE: ~5 kcal/mol, RMSE: 9–10 kcal/mol; Table 10). These observations suggest that there is no significant overfitting of the parameters and that the new PM7 is broadly applicable to Ag clusters within the size range used in the training and test sets.

3.4. Performance of Parameters for Larger Ag Clusters. To this point, all of our results have focused on Ag clusters within the size range included in the training set (2-7 Ag atoms). Here, we examine the performance of our new PM7 parameters for Ag clusters of 8-15 atoms, up to about twice the size of the clusters in the training set. This tests versatility of the parameters to produce reasonable results for systems that are not directly comparable to structures in the training set. For reasons of computational cost, it is impractical to perform CCSD(T) calculations to generate ground-state PESs for larger Ag clusters. Instead, we use DFT-based reference data at the M06/ECP28MWB level.⁵⁴ The M06 functional has previously been shown to produce accurate relative energies of Ag_n clusters with $3 \le n \le 8$ compared to CCSD(T),63 and our results similarly showed that the M06/ ECP28MWB level of theory yields an RMSE of 0.76 kcal/mol for relative energies of Ag_n clusters with $3 \le n \le 7$ (Table 5). Since our new PM7 parameters performed better than M06/ ECP28MWB for binding energies of small clusters, it is not reasonable to use this level of theory as the reference data for binding energies of larger clusters. Therefore, only the relative energies are considered in this test. Our reference data set contains the M06/ECP28MWB-optimized geometries and energies of all isomers of Ag_n ($8 \le n \le 15$) with charges of -1, 0, and +1 from McKee and Samokhvalov,⁵⁴ which yield a total of 153 clusters. Since Ag_{10} and Ag_{11} in their data set do not contain structural isomers, they cannot be used to compute relative energies. Hence, a total of six structures were excluded for this test. The errors in relative energies are computed as the deviation from the average energy of structures with the same empirical formula as shown in eq 7, and the MSE is not reported because it is zero by definition.

For these larger clusters, the new PM7 parameters are more accurate than the default PM7 by a factor of about 1.5 and more accurate than PM6 by a factor of 3.5 (Table 11). Across the full size range ($8 \le n \le 15$), the new PM7 parameters have an RMSE of 13.97 kcal/mol, which is larger than the value of 4.41 for clusters of 2–7 atoms, indicating that the parameters are somewhat less accurate for the larger Ag clusters. To understand the origins of this increase in error, we also decompose the relative energy data into two groups based on size: Ag_8-Ag_{12} and $Ag_{13}-Ag_{15}$ (Table 11). The errors in both size ranges are larger than those seen in the training set, but our new parameters have errors around 4 kcal/mol lower errors in the Ag_8-Ag_{12} clusters than in the $Ag_{13}-Ag_{15}$ clusters.

Table 11. Error Statistics (kcal/mol) for the Relative Energies of Isomers of Ag_n ($8 \le n \le 15$) with Decompositions by Size at the New PM7, Default PM7, and PM6 Levels^b

	relative energy, Ag ₈ –Ag ₁₅			
	new PM7	default PM7	PM6	
MAE	10.14	14.12	35.77	
RMSE	13.97	19.47	48.66	
no. of SCF failure	0	1*	0	
	relative energy, A	g_8 -A g_{12}		
	new PM7	default PM7	PM6	
MAE	8.55	12.59	31.16	
RMSE	11.40	19.15	50.96	
no. of SCF failure	0	1 ^a	0	
	relative energy, Ag	g_{13} -A g_{15}		
	new PM7	default PM7	PM6	
MAE	11.01	14.92	38.29	
RMSE	15.19	19.64	47.36	
no. of SCF failure	0	0	0	

^aSince one of two Ag_8^+ isomers had an SCF failure, relative energies are undefined for Ag_8^+ and are excluded from the error statistics. ^bGeometries with SCF failures were excluded when computing the error statistics.

This suggests that the new parameters gradually lose accuracy as the system size deviates from the size of the training set. In contrast, the default PM7 and PM6 yield large errors in both size ranges without clear trends in accuracy with size. Decomposition of the errors by charge and by spin (Tables S5 and S6) shows trends that are quite consistent with the training set: the errors are the smallest for anionic clusters and open-shell clusters, with differences of a few kcal/mol between different charges and spins. This shows that the chemical trends in the performance of our parameters extend to larger clusters.

There are several potential sources for this increase in error. First, our training set included a small number of relative energies since many of the clusters with 2-7 atoms have only one or two stable isomers; thus, relative energies may still be somewhat underweighted in the training set despite using a weight of 80.0. In addition, the Ag clusters with 8-15 atoms typically have a larger number of isomers and span a larger energy range. For example, only six chemical formulas in our training set have more than two isomers, and Ag7 has one of the largest number of structures with six isomers within an energy range 14 kcal/mol. In contrast Ag₁₄ has 14 isomers spanning an energy range of 37 kcal/mol. Consequently, predicting their relative energies accurately is more challenging than for the smaller clusters. Finally, since we only directly compared the M06/ECP28MWB energies to CCSD(T) for up to seven Ag atoms, it is not known whether it maintains such a high level of accuracy in larger clusters with more isomers. Even though the magnitude of the error in relative energy increases with an increasing Ag cluster size, our new Ag parameters significantly reduce errors relative to the default PM7 and PM6 methods.

3.5. Performance of New Parameters in Geometry Optimization. To further examine the versatility of our new parameters, we test their performance in geometry optimization in Ag clusters relative to the set of M06 structures for Ag₈–Ag₁₅ from McKee and Samokhvalov used in the previous

ı

section for benchmarking of relative energies.⁵⁴ Utilizing the Kabsch algorithm to compute the RMSD in the atomic positions between two geometries, we can test how well the new parameters are able to treat geometries with sizes larger than the training data. For simplicity, we compare only the two sets of PM7 parameters. Since PM6 consistently performed poorly for the energetic properties of Ag clusters and has been shown to perform worse than PM7 for Au cluster geometries, we expect PM6 to also perform poorly here.⁶⁵

The average RMSD for all 159 clusters is 0.2608 Å for the new PM7 parameters, which is about a factor of 5 lower than the average RMSD of 1.1739 Å for the default PM7 parameters. This level of improved accuracy is consistent with the improvement in energetic properties we observed in both the training and test sets. The distribution of geometric errors is shown in Figure 4. The new parameters produce

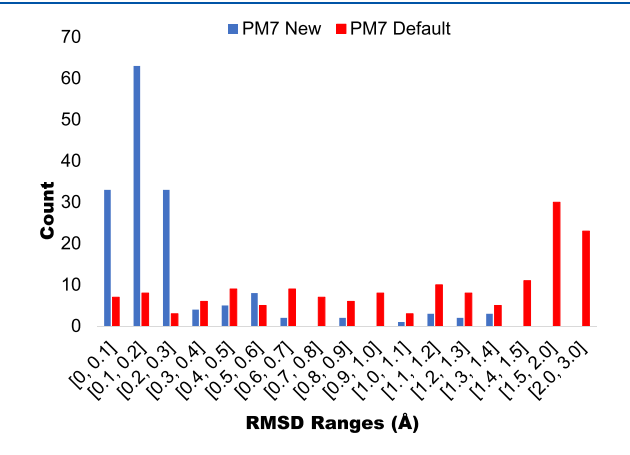


Figure 4. Combined histogram for the RMSD in geometry from new and default PM7 parameters. One SCF failure in default PM7 parameters was excluded from the statistics. Note that the bin width is not uniform after 1.4.

RMSDs smaller than 0.2 Å for 60.4% of the tested geometries and smaller than 0.3 Å for 81.1% of the geometries; only 5.6% of the geometries have errors larger than 1.0 Å. Additionally, none of the geometries produced by our new parameters have RMSDs larger than 1.4 Å. Since the RMSD is calculated based on the atomic positions, 57,58 a lower RMSD indicates less deviation in the structure of the new geometry compared to the reference geometry. Decomposition by cluster size shows no obvious scaling of error magnitude as size increases. For all cluster sizes within the range studied, most structures have RMSDs smaller than 0.3 Å (see Figure S2 in the Supporting Information). On the other hand, the default parameters produce very large errors for a large number of geometries. The default parameters generate RMSDs larger than 1.0 Å for 56.6% of the tested geometries, which is 10 times as many as for the new parameters, and larger than 2.0 Å (with many of them close to 3.0 Å) for 14.5% of the total geometries. The individual RMSD for each geometry can be found in Table S7 in the Supporting Information.

To show more clearly the relationship between RMSD and geometric accuracy, two examples of Ag cluster geometries are shown in Figure 5. Our new parameters retain the basic 3D structure of the M06 reference geometry, with minor differences in bond lengths and angles. All of the labeled bonds in these structures change in length by less than 0.15 Å upon reoptimization, and many bonds undergo much smaller

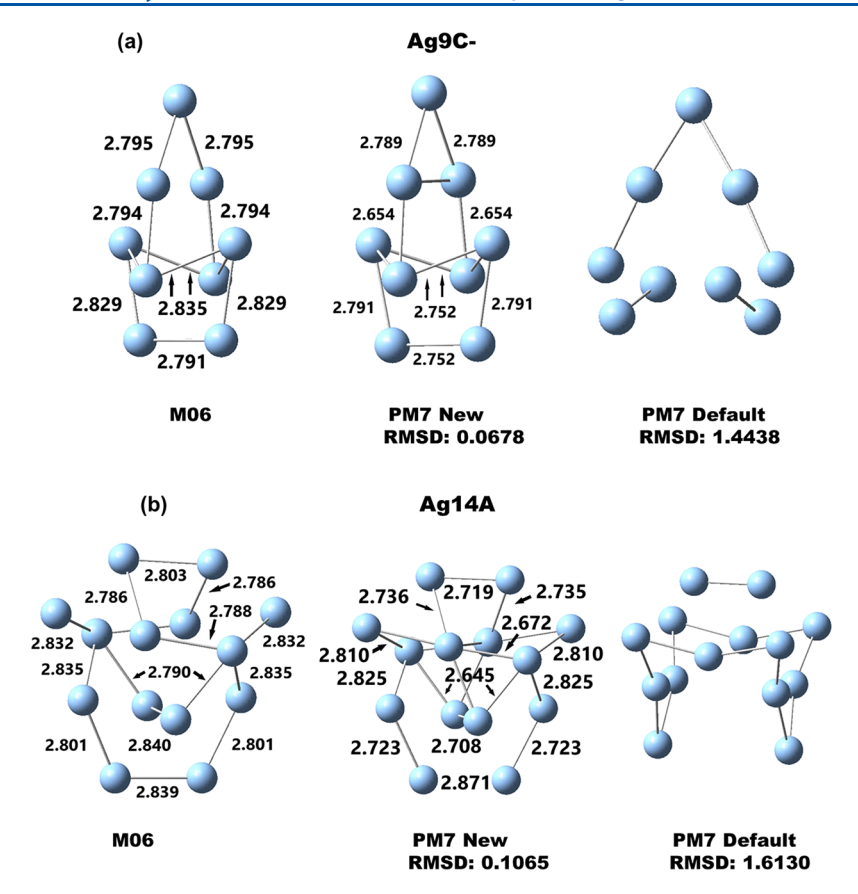


Figure 5. Two representative examples of geometry optimization from the new and default PM7, with their M06 geometries as references. Panel (a) is for an anionic Ag_9 cluster, and panel (b) is for a neutral Ag_{14} cluster. Major bond lengths (in Å) are mapped out based on the M06 reference geometry. Default PM7 structures do not resemble the reference geometry, so bond length measurements are omitted.

changes. Some bonds are lengthened and some are shortened, suggesting that the new PM7 parameters produce fairly small systematic errors in Ag—Ag bond lengths. In contrast, the default PM7 parameters result in geometries with 3D structures very different from the M06 geometries. These results suggest that incorporating PES data into the training set produces parameters that can be used for geometry optimization, even for structures outside the training set.

4. CONCLUSIONS

Accurate semiempirical quantum mechanical models for metals can aid in understanding the chemical properties of these systems at accessible computational costs. Here, we have reparametrized the PM7 semiempirical method to reproduce the ground-state potential energy surfaces of Ag clusters. Our training set contained a total of 1795 single-point energies of Ag_n clusters ($2 \le n \le 7$) at the CCSD(T) level, including both equilibrium and displaced geometries. The parametrization was performed using a procedure based on a genetic algorithm.

The new PM7 parameters produced using this procedure yield a weighted RMSE of 11.28 kcal/mol for the training set. The new parameters reduce the overall error by about a factor of 5 relative to the default PM7 parameters and a factor of 9 relative to PM6. These parameters significantly reduce the error across all of the properties we have examined: binding energy, change in energy upon displacement from an equilibrium geometry, and relative energy between isomers. The errors in the binding energies for equilibrium geometries are even smaller than those of the DFT functional M06, which

has been shown previously to be one of the most accurate functionals for Ag clusters. 62,63 Our new parameters are reasonably accurate across the full scope of chemical structures in the training set and tend to be slightly more accurate for anionic or open-shell clusters and for geometries close to equilibrium. Analysis of the three categories within the test set shows no signs of overfitting. The new parameters also improve the accuracy of the relative isomer energies of larger Ag_n clusters ($8 \le n \le 15$) compared to the reference data computed using the M06 functional, showing that these parameters are applicable to clusters beyond the size range of the training set.

Our PM7 parameters provide a new option to study Ag nanoclusters theoretically at low computational cost with reasonable accuracy. Low-cost methods have particular value for studying properties like dynamics that require computing a large number of time steps. To our knowledge, our parameter set is the first Hartree-Fock-based semiempirical method to yield even qualitatively accurate ground-state energies and potential energy surfaces for clusters of a noble metal. This demonstrates that semiempirical methods have great promise for metals, which have been underexplored using low-cost computational methods. We believe this parametrization approach can be extended to a wide range of metal clusters and complexes and, in particular, to ligand-protected clusters and clusters interacting with molecules of interest for applications like catalysis. These efforts will greatly broaden the scope of chemical applications for semiempirical quantum mechanical methods.

ASSOCIATED CONTENT

Supporting Information

The Supporting Information is available free of charge at https://pubs.acs.org/doi/10.1021/acs.jpca.2c05782.

Cartesian coordinates of all equilibrium geometries of Ag_n clusters $(2 \le n \le 7)$; energies of all structures in the training set, test set, and larger Ag cluster set; decomposition of larger Ag cluster errors by size and charge; and errors in geometry optimization for the larger Ag clusters (PDF)

Cartesian coordinates of the Ag clusters in the study (ZIP)

AUTHOR INFORMATION

Corresponding Author

Rebecca L. M. Gieseking — Department of Chemistry, Brandeis University, Waltham, Massachusetts 02453, United States; orcid.org/0000-0002-7343-1253; Phone: (781)-736-2511; Email: gieseking@brandeis.edu

Author

Qiwei Sun — Department of Chemistry, Brandeis University, Waltham, Massachusetts 02453, United States;
orcid.org/0000-0001-9938-817X

Complete contact information is available at: https://pubs.acs.org/10.1021/acs.jpca.2c05782

Notes

The authors declare no competing financial interest.

ACKNOWLEDGMENTS

The authors would like to thank Elyse Hahn for assistance in generating reference data and Alva Dillion for useful discussions. This work was supported by an NSF CAREER award (CHE-2046099). Computational work was performed on the Brandeis HPCC, which is partially supported by the NSF through DMR-MRSEC 2011846 and OAC-1920147.

REFERENCES

- (1) Du, Y.; Sheng, H.; Astruc, D.; Zhu, M. Atomically Precise Noble Metal Nanoclusters as Efficient Catalysts: A Bridge between Structure and Properties. *Chem. Rev.* **2020**, *120*, 526–622.
- (2) Zhu, J.; Hu, L.; Zhao, P.; Lee, L. Y. S.; Wong, K.-Y. Recent Advances in Electrocatalytic Hydrogen Evolution Using Nanoparticles. *Chem. Rev.* **2020**, *120*, 851–918.
- (3) Gellé, A.; Jin, T.; de la Garza, L.; Price, G. D.; Besteiro, L. V.; Moores, A. Applications of Plasmon-Enhanced Nanocatalysis to Organic Transformations. *Chem. Rev.* **2020**, *120*, 986–1041.
- (4) Chakraborty, I.; Pradeep, T. Atomically Precise Clusters of Noble Metals: Emerging Link between Atoms and Nanoparticles. *Chem. Rev.* **2017**, *117*, 8208–8271.
- (5) Meng, X.; Liu, L.; Ouyang, S.; Xu, H.; Wang, D.; Zhao, N.; Ye, J. Nanometals for Solar-to-Chemical Energy Conversion: From Semi-conductor-Based Photocatalysis to Plasmon-Mediated Photocatalysis and Photo-Thermocatalysis. *Adv. Mater.* **2016**, *28*, 6781–6803.
- (6) Jin, R.; Zeng, C.; Zhou, M.; Chen, Y. Atomically Precise Colloidal Metal Nanoclusters and Nanoparticles: Fundamentals and Opportunities. *Chem. Rev.* **2016**, *116*, 10346–10413.
- (7) Eckhardt, S.; Brunetto, P. S.; Gagnon, J.; Priebe, M.; Giese, B.; Fromm, K. M. Nanobio Silver: Its Interactions with Peptides and Bacteria, and Its Uses in Medicine. *Chem. Rev.* **2013**, *113*, 4708–4754.
- (8) Gonzàlez-Rosell, A.; Cerretani, C.; Mastracco, P.; Vosch, T.; Copp, S. M. Structure and Luminescence of DNA-Templated Silver Clusters. *Nanoscale Adv.* **2021**, *3*, 1230–1260.

- (9) Joshi, C. P.; Bootharaju, M. S.; Bakr, O. M. Tuning Properties in Silver Clusters. *J. Phys. Chem. Lett.* **2015**, *6*, 3023–3035.
- (10) Morton, S. M.; Silverstein, D. W.; Jensen, L. Theoretical Studies of Plasmonics Using Electronic Structure Methods. *Chem. Rev.* **2011**, *111*, 3962–3994.
- (11) Trindell, J. A.; Duan, Z.; Henkelman, G.; Crooks, R. M. Well-Defined Nanoparticle Electrocatalysts for the Refinement of Theory. *Chem. Rev.* **2020**, *120*, 814–850.
- (12) Alkis, S.; Krause, J. L.; Fry, J. N.; Cheng, H.-P. Dynamics of Ag Clusters on Complex Surfaces: Molecular Dynamics Simulations. *Phys. Rev. B* **2009**, 79, No. 121402.
- (13) Guo, J. Y.; Xu, C. X.; Hu, A. M.; Oakes, K. D.; Sheng, F. Y.; Shi, Z. L.; Dai, J.; Jin, Z. L. Sintering Dynamics and Thermal Stability of Novel Configurations of Ag Clusters. *J. Phys. Chem. Solids* **2012**, *73*, 1350–1357.
- (14) Li, H.-S.; Wei, D.; Zhao, X.; Ren, X.; Zhang, D.; Ju, W. Thermal Stability of Ag13— Clusters Studied by Ab Initio Molecular Dynamics Simulations. *J. Phys. Chem. A* **2020**, *124*, 4325—4332.
- (15) Kuda-Singappulige, G. U.; Aikens, C. M. Excited-State Absorption in Silver Nanoclusters. *J. Phys. Chem. C* **2021**, 125, 24996–25006.
- (16) Chen, B. W. J.; Xu, L.; Mavrikakis, M. Computational Methods in Heterogeneous Catalysis. *Chem. Rev.* **2021**, *121*, 1007–1048.
- (17) Jena, P.; Sun, Q. Super Atomic Clusters: Design Rules and Potential for Building Blocks of Materials. *Chem. Rev.* **2018**, *118*, 5755–5870.
- (18) Thiel, W. Semiempirical Quantum—Chemical Methods. Wiley Interdiscip. Rev.: Comput. Mol. Sci. 2014, 4, 145–157.
- (19) Christensen, A. S.; Kubař, T.; Cui, Q.; Elstner, M. Semiempirical Quantum Mechanical Methods for Noncovalent Interactions for Chemical and Biochemical Applications. *Chem. Rev.* **2016**, *116*, 5301–5337.
- (20) Bowler, D. R.; Miyazaki, T. O(N) Methods in Electronic Structure Calculations. *Rep. Prog. Phys.* **2012**, *75*, No. 036503.
- (21) Giese, T. J.; Sherer, E. C.; Cramer, C. J.; York, D. M. A Semiempirical Quantum Model for Hydrogen-Bonded Nucleic Acid Base Pairs. *J. Chem. Theory Comput.* **2005**, *1*, 1275–1285.
- (22) Soyemi, A.; Szilvási, T. Benchmarking Semiempirical QM Methods for Calculating the Dipole Moment of Organic Molecules. *J. Phys. Chem. A* **2022**, *126*, 1905–1921.
- (23) Wu, X.; Thiel, W.; Pezeshki, S.; Lin, H. Specific Reaction Path Hamiltonian for Proton Transfer in Water: Reparameterized Semiempirical Models. *J. Chem. Theory Comput.* **2013**, *9*, 2672–2686.
- (24) Gieseking, R. L.; Ratner, M. A.; Schatz, G. C. Semiempirical Modeling of Ag Nanoclusters: New Parameters for Optical Property Studies Enable Determination of Double Excitation Contributions to Plasmonic Excitation. *J. Phys. Chem. A* **2016**, 120, 4542–4549.
- (25) Gieseking, R. L.; Ratner, M. A.; Schatz, G. C. Theoretical Modeling of Voltage Effects and the Chemical Mechanism in Surface-Enhanced Raman Scattering. *Faraday Discuss.* **2017**, 205, 149–171.
- (26) Gieseking, R. L. M. A New Release of MOPAC Incorporating the INDO/S Semiempirical Model with CI Excited States. *J. Comput. Chem.* **2021**, 42, 365–378.
- (27) Dral, P. O.; Wu, X.; Spörkel, L.; Koslowski, A.; Weber, W.; Steiger, R.; Scholten, M.; Thiel, W. Semiempirical Quantum-Chemical Orthogonalization-Corrected Methods: Theory, Implementation, and Parameters. J. Chem. Theory Comput. 2016, 12, 1082—1096.
- (28) Dral, P. O.; Wu, X.; Spörkel, L.; Koslowski, A.; Thiel, W. Semiempirical Quantum-Chemical Orthogonalization-Corrected Methods: Benchmarks for Ground-State Properties. *J. Chem. Theory Comput.* **2016**, *12*, 1097–1120.
- (29) Elstner, M.; Seifert, G. Density Functional Tight Binding. *Philos. Trans. R. Soc., A* **2014**, 372, 20120483.
- (30) Cuny, J.; Tarrat, N.; Spiegelman, F.; Huguenot, A.; Rapacioli, M. Density-Functional Tight-Binding Approach for Metal Clusters, Nanoparticles, Surfaces and Bulk: Application to Silver and Gold. *J. Phys.: Condens. Matter* **2018**, *30*, 303001.

- (31) Oliveira, L. F. L.; Tarrat, N.; Cuny, J.; Morillo, J.; Lemoine, D.; Spiegelman, F.; Rapacioli, M. Benchmarking Density Functional Based Tight-Binding for Silver and Gold Materials: From Small Clusters to Bulk. *J. Phys. Chem. A* **2016**, *120*, 8469–8483.
- (32) Alkan, F.; Aikens, C. M. TD-DFT and TD-DFTB Investigation of the Optical Properties and Electronic Structure of Silver Nanorods and Nanorod Dimers. *J. Phys. Chem. C* **2018**, *122*, 23639–23650.
- (33) Cui, Q.; Elstner, M. Density Functional Tight Binding: Values of Semi-Empirical Methods in an Ab Initio Era. *Phys. Chem. Chem. Phys.* **2014**, *16*, 14368–14377.
- (34) Bannwarth, C.; Ehlert, S.; Grimme, S. GFN2-XTB—An Accurate and Broadly Parametrized Self-Consistent Tight-Binding Quantum Chemical Method with Multipole Electrostatics and Density-Dependent Dispersion Contributions. *J. Chem. Theory Comput.* **2019**, *15*, 1652–1671.
- (35) Maurer, L. R.; Bursch, M.; Grimme, S.; Hansen, A. Assessing Density Functional Theory for Chemically Relevant Open-Shell Transition Metal Reactions. *J. Chem. Theory Comput.* **2021**, *17*, 6134–6151.
- (36) Stewart, J. J. P. Optimization of Parameters for Semiempirical Methods V: Modification of NDDO Approximations and Application to 70 Elements. *J. Mol. Model.* **2007**, *13*, 1173–1213.
- (37) Stewart, J. J. P. Optimization of Parameters for Semiempirical Methods VI: More Modifications to the NDDO Approximations and Re-Optimization of Parameters. *J. Mol. Model.* **2013**, *19*, 1–32.
- (38) Stewart, J. J. P. Comparison of Structures of 70 Silver-containing Solids predicted using PM7 and PM6-D3H4 with X-Ray. http://openmopac.net/PM7_and_PM6-D3H4_accuracy/Ag.html (accessed 2022-04-15).
- (39) Stewart, J. J. P. Accuracy of PM7 and PM6-D3H4. http://openmopac.net/PM7_and_PM6-D3H4_accuracy/Accuracy%20of%20PM7%20and%20PM6-D3H4.html (accessed 2022-04-15).
- (40) Gieseking, R. L. M.; Ratner, M. A.; Schatz, G. C. Benchmarking Semiempirical Methods To Compute Electrochemical Formal Potentials. *J. Phys. Chem. A* **2018**, *122*, 6809–6818.
- (41) Brothers, E. N.; Merz, K. M. Sodium Parameters for AM1 and PM3 Optimized Using a Modified Genetic Algorithm. *J. Phys. Chem.* B 2002, 106, 2779–2785.
- (42) Fredin, L. A.; Allison, T. C. Predicting Structures of Ru-Centered Dyes: A Computational Screening Tool. *J. Phys. Chem. A* **2016**, *120*, 2135–2143.
- (43) Dutra, J. D. L.; Filho, M. A. M.; Rocha, G. B.; Freire, R. O.; Simas, A. M.; Stewart, J. J. P. Sparkle/PM7 Lanthanide Parameters for the Modeling of Complexes and Materials. *J. Chem. Theory Comput.* **2013**, *9*, 3333–3341.
- (44) Becke, A. D. Density-Functional Exchange-Energy Approximation with Correct Asymptotic Behavior. *Phys. Rev. A* **1988**, *38*, 3098–3100
- (45) Stephens, P. J.; Devlin, F. J.; Chabalowski, C. F.; Frisch, M. J. Ab Initio Calculation of Vibrational Absorption and Circular Dichroism Spectra Using Density Functional Force Fields. *J. Phys. Chem.* **1994**, *98*, 11623–11627.
- (46) Grimme, S.; Antony, J.; Ehrlich, S.; Krieg, H. A Consistent and Accurate Ab Initio Parametrization of Density Functional Dispersion Correction (DFT-D) for the 94 Elements H-Pu. *J. Chem. Phys.* **2010**, 132, 154104.
- (47) Figgen, D.; Rauhut, G.; Dolg, M.; Stoll, H. Energy-Consistent Pseudopotentials for Group 11 and 12 Atoms: Adjustment to Multi-Configuration Dirac—Hartree—Fock Data. *Chem. Phys.* **2005**, *311*, 227–244.
- (48) Peterson, K. A.; Puzzarini, C. Systematically Convergent Basis Sets for Transition Metals. II. Pseudopotential-Based Correlation Consistent Basis Sets for the Group 11 (Cu, Ag, Au) and 12 (Zn, Cd, Hg) Elements. *Theor. Chem. Acc.* **2005**, *114*, 283–296.
- (49) Pritchard, B. P.; Altarawy, D.; Didier, B.; Gibson, T. D.; Windus, T. L. New Basis Set Exchange: An Open, Up-to-Date Resource for the Molecular Sciences Community. *J. Chem. Inf. Model.* **2019**, *59*, 4814–4820.

- (50) Bartlett, R. J.; Musiał, M. Coupled-Cluster Theory in Quantum Chemistry. *Rev. Mod. Phys.* **2007**, *79*, 291–352.
- (51) Reiher, M. Douglas-Kroll-Hess Theory: A Relativistic Electrons-Only Theory for Chemistry. *Theor. Chem. Acc.* **2006**, *116*, 241–252.
- (52) Zhao, Y.; Truhlar, D. G. The M06 Suite of Density Functionals for Main Group Thermochemistry, Thermochemical Kinetics, Noncovalent Interactions, Excited States, and Transition Elements: Two New Functionals and Systematic Testing of Four M06-Class Functionals and 12 Other Functionals. *Theor. Chem. Acc.* 2008, 120, 215–241.
- (53) Andrae, D.; Häußermann, U.; Dolg, M.; Stoll, H.; Preuß, H. Energy-Adjusted*ab Initio* Pseudopotentials for the Second and Third Row Transition Elements. *Theor. Chim. Acta* **1990**, *77*, 123–141.
- (54) McKee, M. L.; Samokhvalov, A. Density Functional Study of Neutral and Charged Silver Clusters Ag_n with n = 2-22. Evolution of Properties and Structure. *J. Phys. Chem. A* **2017**, *121*, 5018–5028.
- (55) Frisch, M. J.; Trucks, G. W.; Schlegel, H. B.; Scuseria, G. E.; Robb, M. A.; Cheeseman, J. R.; Scalmani, G.; Barone, V.; Mennucci, B.; Petersson, G. A., et al.. *Gaussian 16, Revision B.01*; Gaussian, Inc.: Wallingford CT, 2016.
- (56) Stewart, J. J. P. MOPAC: A Semiempirical Molecular Orbital Program. J. Comput.-Aided Mol. Des. 1990, 4, 1–103.
- (57) Calculate Root-mean-square deviation (RMSD) of Two Molecules Using Rotation, GitHub, http://github.com/charnley/rmsd(accessed 2022-07-15).
- (58) Kabsch, W. A Solution for the Best Rotation to Relate Two Sets of Vectors. *Acta Crystallogr., Sect. A: Found. Adv.* **1976**, 32, 922–923.
- (59) Stewart, J. J. P. Application of the PM6 Method to Modeling the Solid State. J. Mol. Model. 2008, 14, 499.
- (60) Stewart, J. J. P. Average Errors in Heat of Formation, per Element. http://openmopac.net/PM7_and_PM6-D3H4_accuracy/Stats_for_Heats_of_Formation_per_Element.html (accessed 2022-04-15).
- (61) Stewart, J. J. P. Comparison of Structures of 1338 Carbon-containing Solids predicted using PM7 and PM6-D3H4 with X-Ray. http://openmopac.net/PM7_and_PM6-D3H4_accuracy/C.html (accessed 2022-04-15).
- (62) Duanmu, K.; Truhlar, D. G. Validation of Methods for Computational Catalyst Design: Geometries, Structures, and Energies of Neutral and Charged Silver Clusters. *J. Phys. Chem. C* **2015**, *119*, 9617–9626.
- (63) Chen, M.; Dyer, J. E.; Li, K.; Dixon, D. A. Prediction of Structures and Atomization Energies of Small Silver Clusters, (Ag)n, n < 100. *J. Phys. Chem. A* **2013**, *117*, 8298–8313.
- (64) Baek, H.; Moon, J.; Kim, J. Benchmark Study of Density Functional Theory for Neutral Gold Clusters, Aun (n = 2-8). *J. Phys. Chem. A* **2017**, *121*, 2410–2419.
- (65) Mato, J.; Guidez, E. B. Accuracy of the PM6 and PM7 Methods on Bare and Thiolate-Protected Gold Nanoclusters. *J. Phys. Chem. A* **2020**, *124*, 2601–2615.